

Cite this: *J. Mater. Chem. A*, 2020, **8**, 15936

Enhancing CO₂ reduction by suppressing hydrogen evolution with polytetrafluoroethylene protected copper nanoneedles†

Pengda An,^{ab} Lai Wei,^a Huangjingwei Li,^a Baopeng Yang,^a Kang Liu,^a Junwei Fu,^a Hongmei Li,^a Hui Liu,^c Junhua Hu,^d Ying-Rui Lu,^e Hao Pan,^f Ting-Shan Chan,^{*g} Ning Zhang^{ib}*^b and Min Liu^{ib}*^a

With the fast development of society and industry, atmospheric levels of carbon dioxide (CO₂) have increased seriously, becoming a threat to the world's climate. Electrochemical transformation of CO₂ into fuels and chemicals using copper (Cu)-based materials has attracted enormous attention. However, the competitive hydrogen evolution reaction (HER) heavily influences their efficiency. Thus, it is urgent to promote the CO₂ reduction reaction (CO₂RR) and suppress the competitive HER. In this work, enhanced CO₂RR with suppressed HER was achieved on polytetrafluoroethylene (PTFE) coated Cu nanoneedles (CuNNs). The concentration of surface adsorbed CO₂ could be enhanced *via* the field-induced reagent concentration (FIRC) effect through the CuNN structures. The hydrophobic PTFE can prevent the supply of protons to CuNNs and thus suppress the HER. Scanning electron microscopy (SEM), transmission electron microscopy (TEM), and X-ray absorption spectroscopy (XAS) revealed that the PTFE coated CuNNs maintained the nanoneedle structures and metallic Cu state during the catalytic reaction process. As a result, highly suppressed HER coupled with high C₂ selectivity can be achieved on these PTFE coated CuNNs with a Faraday efficiency (FE) of 47% toward C₂ products and an ultralow FE of 5.9% toward H₂ at -1.49 V vs. RHE (without IR correction). This work provides an effective strategy to promote the CO₂RR and suppress the competitive HER.

Received 2nd April 2020
Accepted 14th May 2020

DOI: 10.1039/d0ta03645e

rsc.li/materials-a

1. Introduction

Electrochemical reduction of CO₂ to useful fuels has been widely studied as it is a feasible approach to handle the rising atmospheric CO₂ concentration and integrate renewable intermittent energy, such as wind and solar energy, into useful chemicals.¹⁻⁴ Many kinds of materials were studied for the CO₂RR;⁵⁻⁷ however, metals such as gold,⁸ tin,⁹ copper,¹⁰⁻¹⁵ and their derivatives are the most common and attractive materials among catalysts for the CO₂RR. Cu-based materials have been widely investigated because Cu is the only metal that can

generate considerable amounts of C₂₊ products such as ethylene (C₂H₄), ethanol (C₂H₅OH) and propanol (C₃H₇OH).^{16,17} To enhance the FE of more valuable C₂₊ products, a lot of attention has been focused on regulating exposed facets,¹⁸ surface pH,¹⁹ subsurface O²⁻ and residual oxidation states.^{20,21} Although a high C₂₊ FE of over 50% has been reached, the FE of the competing reaction, HER, remains in the range of 20–30%.

An important reason for hydrogen generation in large quantities during CO₂RR in aqueous solution is the HER occurs with a lower overpotential and a negligible limitation of mass transfer.²² In contrast, the CO₂RR is always restricted by the large kinetic overpotential caused by the low concentration of CO₂ surrounding the catalytic site.²²⁻²⁴ This results in the inevitable hydrogen generation during the CO₂RR in aqueous electrolytes. Increasing the concentration of CO₂ is a feasible approach to solve the above-mentioned problem. Some effort has been made to promote the solubility of CO₂ in reaction systems such as testing under high pressure,²⁵ employing ionic liquids with organic solvents,²⁶ etc. However, these routes are not universal and expensive.

Recently, the promoting effect of a sharp tip electrode on the CO₂RR has been proved theoretically²⁷ and experimentally.^{24,28,29} Sharp tips cause local high electric field and electrons will selectively gravitate toward areas of high curvature. The electric field caused by concentrated electrons attracted increased K⁺

^aState Key Laboratory of Powder Metallurgy, School of Physics and Electronics, Central South University, Changsha, 410083, Hunan, China. E-mail: minliu@csu.edu.cn

^bSchool of Materials Science and Engineering, Central South University, Changsha 410083, Hunan, China. E-mail: nzhang@csu.edu.cn

^cSchool of Metallurgy and Environment, Central South University, Changsha 410083, Hunan, China

^dSchool of Materials Science and Engineering, Zhengzhou University, Zhengzhou 450002, Henan, China

^eNational Synchrotron Radiation Research Center, Hsinchu, 30076, Taiwan. E-mail: chan.ts@nsrc.org.tw

^fDepartment of Periodontics & Oral Mucosal Section, Xiangya Stomatological Hospital, Central South University, 72 Xiangya Road, Changsha, Hunan, China

† Electronic supplementary information (ESI) available. See DOI: 10.1039/d0ta03645e

around the tip, which can increase the concentration of CO_2 .^{24,28,30} To further suppress the competitive HER, we hypothesize that using a hydrophobic thin layer to prevent the supply of protons to a Cu nanoneedle electrode but allow CO_2 to the electrode would be a potential approach to enhance the CO_2RR and suppress the HER.^{31,32}

In this work, we report that PTFE-coated CuNNs could concentrate electrons and K^+ ions to enhance the concentration of CO_2 near the tips and prevent the supply of protons to the electrode. The SEM and TEM images proved the PTFE was uniformly coated on CuNNs, which maintained the needle morphology during the reaction. The metallic Cu state was confirmed by X-ray photoelectron spectroscopy (XPS) and XAS. COMSOL simulation and ion chromatography (IC) measurement revealed that CuNNs could concentrate K^+ and thus CO_2 molecules. Contact angle tests showed the PTFE coated CuNNs had better hydrophobic properties. Therefore, the obtained sample exhibited suppressed HER and enhanced CO_2RR performances with a remarkable H_2 FE of as low as 5.9% and a high C_2 FE of 47% at -1.49 V vs. RHE.

2. Result and discussion

2.1 Characterization of the as-obtained catalysts

The preparation process of CuNNs is schematically illustrated in Fig. 1a. The CuNNs were prepared by a simple anodization process and covered with PTFE through a simple dipping

method. The SEM images show that bunches of nanoneedles were grown on electrochemically polished Cu foil (Fig. 1b) and PTFE was coated on these CuNNs (Fig. 1f). However, PTFE was not coated on the CuNNs perfectly, and the uncoated regions will act as the active site during the CO_2 reduction test. It can be seen that the bare CuNNs collapsed into curved nanowires (henceforth referred to as CuNWs) after the electrochemical test (Fig. 1c–e). Notably, PTFE covered CuNNs maintained the same morphology after the long term test (Fig. 1g–i). The TEM images further confirmed that CuNNs could maintain the morphology with the PTFE cover and the bare CuNNs were converted into CuNWs (Fig. 1e and i).

Fourier transform infrared spectroscopy (FT-IR) was employed to collect the surface information on the samples. The as-obtained CuNNs (Fig. S1a†) showed multiple peaks in the range of $400\text{--}1000\text{ cm}^{-2}$. After the coating of PTFE (Fig. 2a), two characteristic peaks belonging to PTFE at around 1200 cm^{-2} can be clearly observed. These two peaks remained even after the test, proving that PTFE was coated on the CuNNs stably.

X-ray diffraction (XRD) was employed to analyze the structure of CuNN samples. The XRD pattern of the as-obtained CuNNs (Fig. S1b†) shows three main peaks at 43.3° , 50.4° and 74.1° , corresponding to the face-centered cubic (fcc) Cu (111), (200), and (220) crystal planes, respectively. The minor peaks at 16.7° , 23.8° , 34.1° belong to $\text{Cu}(\text{OH})_2$. After PTFE coating, the XRD pattern (Fig. 2b) remained the same as that of the CuNNs,

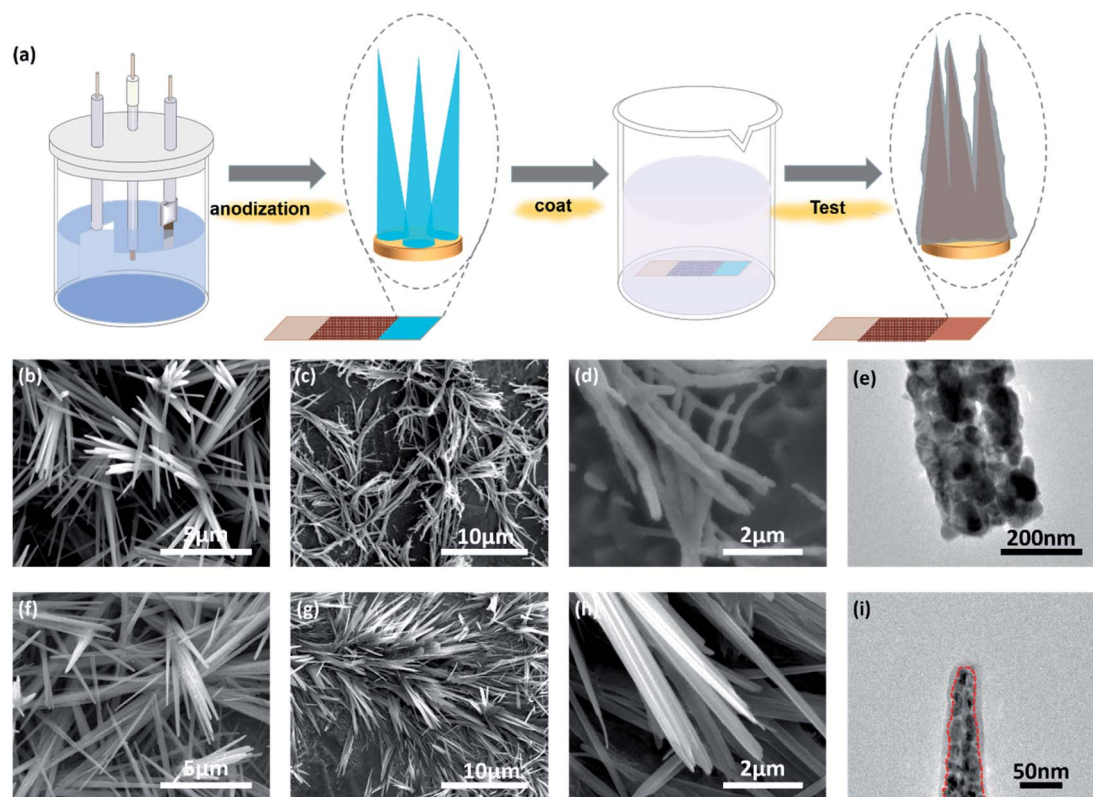


Fig. 1 (a) Schematic illustration of the fabrication of CuNNs. SEM images of CuNWs before the test (b), after the test (c) and with further magnification (d). (e) TEM image of CuNWs after the test. SEM images of CuNNs before the test (f), after the test (g) and with further magnification (h). (i) TEM image of CuNNs after the test.

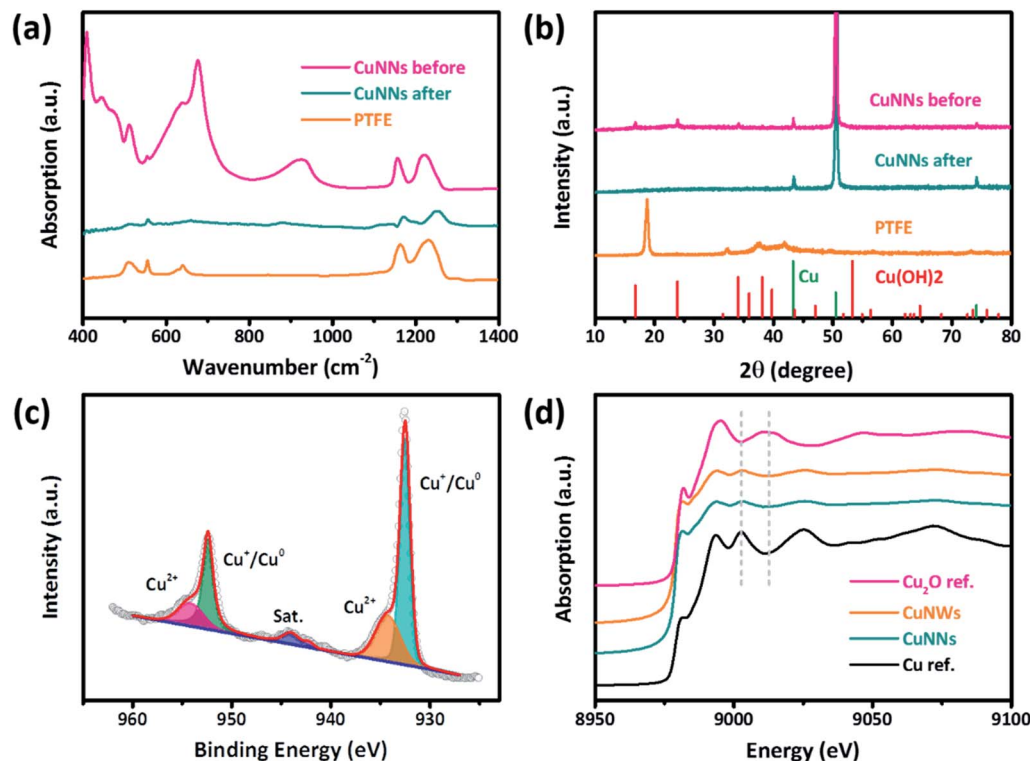


Fig. 2 FT-IR spectrum (a) of CuNNs before the test and after the test and pure PTFE. XRD patterns (b) of CuNNs before the test and after the test and pure PTFE. (c) Cu 2p XPS patterns of CuNNs after the test. (d) Cu K-edge XANES spectra of CuNNs and CuNWs after the electrochemical test.

indicating that the PTFE coating did not affect the structure of CuNNs. After the electrochemical test, the CuNNs showed the characteristic peak of metallic Cu. High resolution TEM (HRTEM) images and selected area electron diffraction (SAED) images confirmed the metallic Cu phases of the obtained CuNNs and CuNWs (Fig. S2[†]).

The chemical states of CuNNs and CuNWs after the CO₂RR were detected by XPS. Both CuNNs (Fig. 2c) and CuNWs (Fig. S3a[†]) showed the metallic state with two peaks at 933.3 and 952.2 eV, corresponding to Cu^{0/+} 2p_{3/2} and Cu^{0/+} 2p_{1/2}, respectively.³³ A minor shoulder peak of Cu²⁺ could be recognized in each band, which was attributed to the oxidation of Cu exposed in air during transportation and tests. The F 1s spectrum proved the presence of PTFE on the CuNNs (Fig. S3b[†]).

X-ray adsorption near edge structure (XANES) was further employed to study the states of the samples. The Cu K-edge of CuNNs and CuNWs after the test (Fig. 2d) exhibited the same characteristic peak at 9005 eV as that of the Cu reference. While, the characteristic peak of Cu₂O was located at 9013 eV.⁴² Based on these results, it can be safely concluded that the CuNNs maintained the metallic state during the CO₂RR process.

2.2 Electrocatalytic performance of CO₂ reduction

To evaluate the electrocatalytic performance for CuNNs, the electrochemical reduction of CO₂ was performed in a typical three-electrode system with Ag/AgCl (3.5 M KCl) as the reference electrode, Pt foil as the counter electrode and CO₂ (>99.999%) saturated 0.1 M KHCO₃ (pH = 6.8) as the electrolyte. It can be

seen that the hydrogen Faraday efficiency (FE(H₂)) of CuNNs was substantially suppressed to a value of 5.9% at −1.49 V vs. RHE (Fig. 3a and S4[†]). This value is only one seventh of 41.6%, FE(H₂) on CuNWs. With the suppression of H₂, FE(CH₄) and FE(C₂H₅OH) are significantly improved, from 4.3% and 7.7% on CuNWs to 32% and 25.8% on CuNNs, respectively. FE(C₂H₄) and FE(CO) are also increased on CuNNs compared with CuNWs. The total FE(C₂) and FE(C₁) for CuNNs reached 47% and 39.3%.

To further investigate the change of FE between the HER and the CO₂RR, an electrocatalytic test was performed from −1.09 to −1.69 V vs. RHE (Fig. 3b and c). The detailed FEs for all the products at different potentials are shown in Tables S1 and S2.[†] Trace amounts of methanol and *n*-propanol were also detected; they were not taken into account since the quantity was too little. It can be seen that FE(H₂) on CuNNs decreased with the increase in potential, and displayed the lowest value of 5.9% at a potential of −1.49 V vs. RHE. In comparison, H₂ is one of the main products for CuNWs at almost all measured potentials. As a result, the FE(H₂) on CuNNs was much lower than those on CuNWs in the tested potential range. On the other hand, the FE(C₂) on CuNNs was much higher than those on CuNWs, especially at a potential around −1.49 V vs. RHE, which verified the enhanced CO₂RR performance of CuNNs.

To demonstrate the exceptional product selectivity of the CuNNs, we then considered the ratio of FE(C₂)/FE(H₂) at different potentials (Fig. 3d). The ratio for CuNNs was higher than those for CuNWs at all tested potentials, especially at

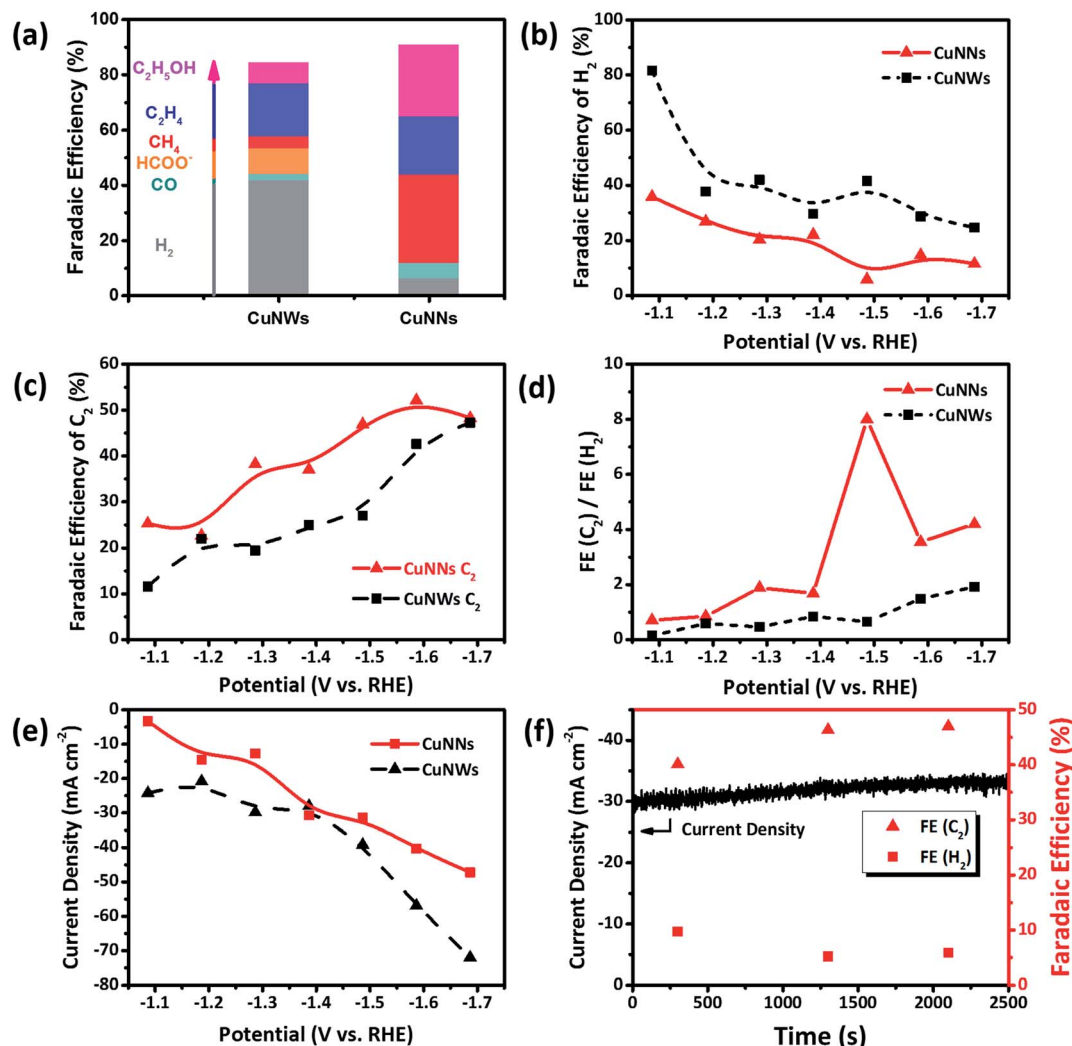


Fig. 3 (a) Product distribution of CuNWs and CuNNs at -1.49 V vs. RHE. FE(H_2) (b) and FE(C_2) (c) of CuNNs and CuNWs at different potentials. (d) The ratio of FE(C_2) and FE(H_2). (e) Current density at different potentials. (f) Stability test of CuNNs at -1.49 V vs. RHE.

-1.49 V vs. RHE with a value of 8 for CuNNs, which was 12.3 times higher than 0.65 for CuNWs. The result indicated that the suppression of the HER and the enhancement of FE(C_2) are achieved simultaneously. The comparison of FE(H_2) and the ratio of FE(C_2)/FE(H_2) with those of other studies is shown in Fig. S5 and Table S3,[†] which demonstrates that CuNNs is one of the best catalysts among Cu-based catalysts studied.

To verify the intrinsic activity of CuNNs, the current density was normalized by ECSA, which was measured by the double layer capacitance method (Fig. S6[†]). The results showed that the normalized current densities of CuNNs were larger than those of CuNWs at the tested potentials (Fig. 3e and S7[†]), confirming the high intrinsic activity of CuNNs. The LSV curves and corresponding Tafel slope are also shown in Fig. S8.[†] The smaller Tafel slope of CuNNs indicated a faster kinetic process.

The stability of CuNNs (Fig. 3f) was evaluated in 0.1 M $KHCO_3$ at -1.49 V vs. RHE. The current density slightly increased, and the FE(H_2) and FE(C_2) were stable during the whole test.

To prove the hydrophobic properties of PTFE, the contact angle of CuNNs was measured (Fig. S9[†]). It can be seen that the CuNNs had a larger contact angle than CuNWs, proving the hydrophobic properties of PTFE. The hydrophobic PTFE could reduce the contact between the electrolyte and Cu, which leads to less adsorbed H^+ and results in less hydrogen generation.^{31,32,34}

2.3 Simulation results

To explore the impact of the nanoneedle morphology on charge behavior at the tip surface, electric field was simulated using COMSOL. The simulation result (Fig. 4a and d) showed that high-curvature CuNNs possess higher surface charge density at the sharp tips than CuNWs since electrons tend to concentrate in the high-curvature area.²⁴ The electrons gathered at the tip of nanoneedles triggered a much higher electric field in the surface than that of CuNWs (Fig. 4b, e and S10[†]). K^+ moves toward the surface of the catalyst under the electric field to maintain the electrostatic balance, which results in more K^+

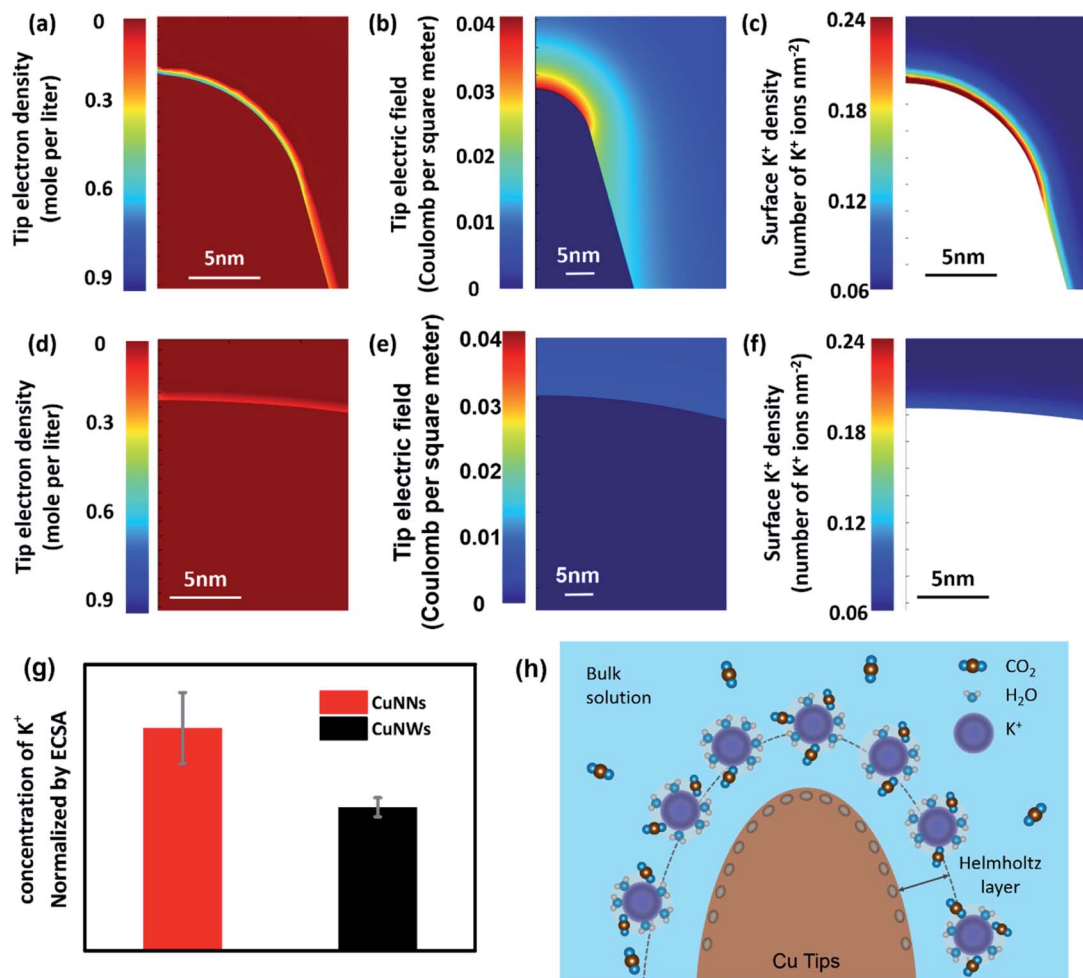


Fig. 4 Free charge density on the surface of CuNNs (a) and CuNWs (d). Electric field distribution near the surface of CuNNs (b) and CuNWs (e). Simulated K^+ concentration on the surface of CuNNs (c) and CuNWs (f). (g) ECSA-normalized field induced concentration of K^+ adsorbed on CuNNs and CuNWs. (h) Schematic diagram of K^+ adsorbed near the surface of the Cu tips.

gathering near the tips of CuNNs than the tips of CuNWs (Fig. 4c and f). The simulated concentration of K^+ near the tip of CuNNs is over 4 times higher than that of CuNWs (Fig. S11†). To prove the enhanced concentration of K^+ adsorbed by CuNNs experimentally, ion chromatography (IC) was employed (Fig. 4g). After keeping the working electrode at -1.49 V vs. RHE for 1.5 minutes, the concentration of K^+ adsorbed on CuNNs is about 2 times higher than that on CuNWs. This electric field induced K^+ concentration phenomenon is schematically represented in Fig. 4h. With the increased CO_2 concentration and decreased protons on the PTFE CuNNs, the CO_2 RR could be much enhanced with greatly suppressed HER.

3. Conclusions

In summary, enhanced CO_2 reduction with suppressed HER was achieved on PTFE coated CuNNs. The faradaic efficiency of H_2 dropped to 5.9%, 7 times lower than that of CuNWs. The selectivity of $FE(C_2)$ and $FE(C_1)$ for CuNNs reached 47% and 39.3%, respectively. The nanoneedle morphology with PTFE was maintained during the test, leading to the FIRC effect.

Concentrated electrons at the tips trigger high concentration of K^+ around the surface, leading to abundant CO_2 at the tips enhancing the efficiency for the CO_2 RR. The hydrophobic PTFE decreased proton supply and suppressed the HER. As a result, the obtained samples showed one of the best ratios of $FE(C_2)/FE(H_2)$ compared to those of reported studies. Our work provides a new insight into promotion of the CO_2 RR by suppressing the competitive HER.

Conflicts of interest

There are no conflicts to declare.

Acknowledgements

This work was supported by the Natural Science Foundation of China (Grant No. 21872174 and U1932148), National Postdoctoral Program for Innovative Talents of China, Postdoctoral Science Foundation of China (Grant No. 2018M640759), Project of Innovation-Driven Plan in Central South University (Grant No. 20180018050001), State Key Laboratory of Powder

Metallurgy, International Science and Technology Cooperation Program (Grant No. 2017YFE0127800 and 2018YFE0203400), Hunan Provincial Science and Technology Program (2017XK2026), Shenzhen Science and Technology Innovation Project (Grant No. JCYJ20180307151313532), Thousand Youth Talents Plan of China and Hundred Youth Talents Program of Hunan, the Hunan Provincial Science and Technology Plan Project (Grant No. 2017TP1001), Ministry of Science and Technology, Taiwan (Contract No. MOST 108-2113-M-213-006), and Outstanding Youth Exchange Program of China Association for Science and Technology (Grant No. 2018CASTQNJL56).

Notes and references

- 1 K. C. S. J. Davis and H. D. Matthews, *Science*, 2010, **329**, 1330–1333.
- 2 L. Zhang, Z. J. Zhao and J. Gong, *Angew. Chem., Int. Ed.*, 2017, **56**, 11326–11353.
- 3 Q. Shen, X. Huang, J. Liu, C. Guo and G. Zhao, *Appl. Catal., B*, 2017, **201**, 70–76.
- 4 Q. Shen, J. Ma, X. Huang, N. Yang and G. Zhao, *Appl. Catal., B*, 2017, **219**, 45–52.
- 5 S. Mou, T. Wu, J. Xie, Y. Zhang, L. Ji, H. Huang, T. Wang, Y. Luo, X. Xiong, B. Tang and X. Sun, *Adv. Mater.*, 2019, **31**, 1903499.
- 6 L. Ji, L. Li, X. Ji, Y. Zhang, S. Mou, T. Wu, Q. Liu, B. Li, X. Zhu, Y. Luo, X. Shi, A. M. Asiri and X. Sun, *Angew. Chem., Int. Ed.*, 2020, **59**, 758–762.
- 7 W. Ju, A. Bagger, G. P. Hao, A. S. Varela, I. Sinev, V. Bon, B. Roldan Cuenya, S. Kaskel, J. Rossmeisl and P. Strasser, *Nat. Commun.*, 2017, **8**, 944.
- 8 Z. Cao, S. B. Zacate, X. Sun, J. Liu, E. M. Hale, W. P. Carson, S. B. Tyndall, J. Xu, X. Liu, X. Liu, C. Song, J. Luo, M. Cheng, X. Wen and W. Liu, *Angew. Chem., Int. Ed.*, 2018, **130**, 12857–12861.
- 9 S. Liu, J. Xiao, X. F. Lu, J. Wang, X. Wang and X. W. D. Lou, *Angew. Chem., Int. Ed.*, 2019, **58**, 8499–8503.
- 10 Q. Zhu, X. Sun, D. Yang, J. Ma, X. Kang, L. Zheng, J. Zhang, Z. Wu and B. Han, *Nat. Commun.*, 2019, **10**, 3851.
- 11 Y. Wang, H. Shen, K. J. T. Livi, D. Raciti, H. Zong, J. Gregg, M. Onadoko, Y. Wan, A. Watson and C. Wang, *Nano Lett.*, 2019, **19**, 8461–8468.
- 12 C. Zou, C. Xi, D. Wu, J. Mao, M. Liu, H. Liu, C. Dong and X. Du, *Small*, 2019, **15**, 1902582.
- 13 K. Xiang, F. Zhu, Y. Liu, Y. Pan, X. Wang, X. Yan and H. Liu, *Electrochem. Commun.*, 2019, **102**, 72–77.
- 14 H. Liu, K. Xiang, Y. Liu, F. Zhu, M. Zou, X. Yan and L. Chai, *ChemElectroChem*, 2018, **5**, 3991–3999.
- 15 J. Zhang, W. Luo and A. Züttel, *J. Mater. Chem. A*, 2019, **7**, 26285–26292.
- 16 J. He, N. J. J. Johnson, A. Huang and C. P. Berlinguette, *ChemSusChem*, 2018, **11**, 48–57.
- 17 X. Chang, A. Malkani, X. Yang and B. Xu, *J. Am. Chem. Soc.*, 2020, **142**, 2975–2983.
- 18 K. Jiang, R. B. Sandberg, A. J. Akey, X. Liu, D. C. Bell, J. K. Nørskov, K. Chan and H. Wang, *Nat. Catal.*, 2018, **1**, 111–119.
- 19 J. J. Lv, M. Jouny, W. Luc, J. H. Zhu and F. Jiao, *Adv. Mater.*, 2018, **30**, 1803111.
- 20 P. D. Luna, R. Quintero-Bermudez, C. Dinh, M. B. Ross, O. S. Bushuyev, P. Todorović, T. Regier, S. O. Kelley, P. Yang and E. H. Sargent, *Nat. Catal.*, 2018, **1**, 103–110.
- 21 Y. Zhou, F. Che, M. Liu, C. Zou, Z. Liang, P. De Luna, H. Yuan, J. Li, Z. Wang, H. Xie, H. Li, P. Chen, E. Bladt, R. Quintero-Bermudez, T. K. Sham, S. Bals, J. Hofkens, D. Sinton, G. Chen and E. H. Sargent, *Nat. Chem.*, 2018, **10**, 974–980.
- 22 D. T. Whipple and P. J. A. Kenis, *J. Phys. Chem. Lett.*, 2010, **1**, 3451–3458.
- 23 C. Kim, T. Möller, J. Schmidt, A. Thomas and P. Strasser, *ACS Catal.*, 2018, **9**, 1482–1488.
- 24 M. Liu, Y. Pang, B. Zhang, P. De Luna, O. Voznyy, J. Xu, X. Zheng, C. T. Dinh, F. Fan, C. Cao, F. P. de Arquer, T. S. Safaei, A. Mepham, A. Klinkova, E. Kumacheva, T. Filleter, D. Sinton, S. O. Kelley and E. H. Sargent, *Nature*, 2016, **537**, 382–386.
- 25 N. Sonoyama, M. Kirii and T. Sakata, *Electrochem. Commun.*, 1999, **1**, 213–216.
- 26 T. N. Huan, P. Simon, G. Rousse, I. Genois, V. Artero and M. Fontecave, *Chem. Sci.*, 2017, **8**, 742–747.
- 27 H. Jiang, Z. Hou and Y. Luo, *Angew. Chem., Int. Ed.*, 2017, **56**, 15617–15621.
- 28 C. Chen, Y. Pang, F. Zhang, J. Zhong, B. Zhang and Z. Cheng, *J. Mater. Chem. A*, 2018, **6**, 19621–19630.
- 29 S. H. Yu, F. Y. Gao, S. J. Hu, X. L. Zhang, Y. R. Zheng, Z. Z. Niu, P. P. Yang, R. C. Bao, T. Ma, Z. Dang, Y. Guan, X. S. Zheng, X. Zheng, J. F. Zhu, M. R. Gao and H. J. Zhang, *Angew. Chem., Int. Ed.*, 2019, **59**, 8706–8712.
- 30 A. Wuttig, Y. Yoon, J. Ryu and Y. Surendranath, *J. Am. Chem. Soc.*, 2017, **139**, 17109–17113.
- 31 Z. Cai, Y. Zhang, Y. Zhao, Y. Wu, W. Xu, X. Wen, Y. Zhong, Y. Zhang, W. Liu, H. Wang, Y. Kuang and X. Sun, *Nano Res.*, 2018, **12**, 345–349.
- 32 Y. Zhang, Z. Cai, Y. Zhao, X. Wen, W. Xu, Y. Zhong, L. Bai, W. Liu, Y. Zhang, Y. Zhang, Y. Kuang and X. Sun, *Nanoscale Horiz.*, 2018, **4**, 490–494.
- 33 J. Kim, W. Choi, J. W. Park, C. Kim, M. Kim and H. Song, *J. Am. Chem. Soc.*, 2019, **141**, 6986–6994.
- 34 D. Wakerley, S. Lamaison, F. Ozanam, N. Menguy, D. Mercier, P. Marcus, M. Fontecave and V. Mougél, *Nat. Mater.*, 2019, **18**, 1222–1227.